Structure dependence of Nb_2O_{5-X} supported manganese oxide for catalytic oxidation of propane: Enhanced oxidation activity for MnO_x on a low surface area Nb_2O_{5-X}

Yixuan Wang[a], Sogand Aghamohammadi[a,b], Danyang Li[c], Kongzhai Li[a,c,*], Robert Farrauto[a,*]

[a] Department of Earth and Environmental Engineering, Columbia University, New York, NY, 10027, USA
[b] Chemical Engineering Faculty, Sahand University of Technology, P.O. Box 51335-1996, Sahand New Town, Tabriz, Iran
[c] Faculty of Metallurgical and Energy Engineering, Kunming University of Science and Technology, Kunming, 650093, China

ARTICLE INFO

ABSTRACT

A series of Nb_2O_{5-x} with different structures were prepared as a carrier to manganese oxide catalysts for total oxidation of propane. The results demonstrated that a monoclinic structure of Nb_2O_{5-x} pre-calcined at 1025 °C, leads to significantly and surprisingly higher catalytic oxidation activity when MnO_x is deposited at 400 °C even with extremely low specific area (around 3.94 m^2/g) relative to the performance of MnO_x/Nb_2O_{5-x} ($\sim$ > 50 m^2/g pre-calcined at 500 °C). Conversion vs temperature profiles for fresh and aged catalysts were generated and performance compared for different materials. Brunauer Emmett Teller (BET) and X-ray diffraction (XRD) were conducted to reveal the textural and structural features of niobium-based catalysts. Raman, X-ray photoelectron spectroscopy (XPS) and temperature programmed reduction (TPR) were performed to further understand the interaction between manganese and niobium oxides. Raman spectra indicated a new Nb-O-Mn species formed due to the strong interaction between the activated niobium oxide carrier at 1025 °C and manganese oxide. This study describes a synergistic catalytic oxidation effect between Mn oxides deposited on a specific phase structure of Nb_2O_{5-x} with very low specific surface area. The enhanced catalytic performance is directly related to the proper ratio of Mn^{3+}/Mn^{4+} coupled with high ratio of Nb^{4+}/Nb^{5+} on the surface and the oxygen vacancies generated between monoclinic Nb_2O_{5-x} and MnO_x.

1. Introduction

It is well known that volatile organic compounds (VOCs) represent a large group of chemicals, toxic to human health due to their mal-odorous, mutagenic and/or carcinogenic nature, but also detrimental to air quality via their role in photochemical smog generation and ozone depletion [1–3]. VOC's emission sources include pharmaceutical and chemical plants, petroleum refineries, automobile manufacturing and transportation fuels, etc. [4]. Consequently, to improve the world's environment and meet the ever-increasing stringent environmental legislation their catalytic abatement has been an active commercial and research topic for many years [5–7].

Propane (C_3H_8) is being produced in great amounts due to extraction of shale gas and liquefied petroleum gas. In addition, the oxidation of propane (C_3H_8) could be considered a prototype pollutant representing volatile organic compounds [8,9]. Accordingly, catalytic materials have been investigated and developed using propane

oxidation as a model compound [5,8,10–12]. It has been reported that supported noble metals (Pt and Pd), perovskite-type catalysts ($LaMnO_3$) and transition metal oxides (Mn, Co, Fe, Cu) are catalytic component for the total oxidation of VOCs [13–17]. However, noble metals are indeed the most active and stable materials but their limited availability and expense are disadvantages which have stimulated the research of alternative non-precious metal oxides. Perovskite-type catalysts show high thermal stability but complicated preparation methods are usually needed to achieve their desired functional structure [14,15]. In contrast, simple transition metal oxides attract interest and exhibit considerably activity and durability but are less active than noble metals [6,8,9].

It has been reported that manganese oxides could offer promising catalytic activity towards the oxidation of propane. For example, Mn_3O_4 and Mn_2O_3 are known for good catalytic activity for catalytic combustion of VOCs [12,13,16,17]. Manganese oxides are also good candidates for total catalytic oxidation of carbon monoxide and the

---

activity among manganese species are reported in the order of $Mn_2O_3 > MnO_2 > MnO$ [18]. Its activity is attributed to the high redox properties and high mobility of lattice oxygen, which can be strongly enhanced by the combination with other metals [13,16–19].

Various high surface area carriers for manganese oxides such as γ-Al_2O_3, TiO_2, SiO_2 and ZrO_2 have been routinely studied. Environmentally friendly niobium oxide has been drawing some attention since it is not only a reducible oxide with oxygen storage capacity [20–23], but also provides a strong metal-support (Nb_2O_5) interaction (SMSI) with catalytic metal oxides altering the oxidation states of catalytic metals [24]. The catalytic properties of niobium compounds have been studied quite extensively [24–31], but none have been used commercially for pollution abatement applications.

A paper from our laboratory by Xiang et al. [30] demonstrated that Nb_2O_5, pre-calcined at 800 °C in air and used as a carrier for cobalt oxide showed remarkably high CO and C_3H_8 oxidation activity and stability relative to cobalt oxides on high surface area Nb_2O_5 or Al_2O_3. Surprisingly comparable behavior to Pt/Al_2O_3 was also reported in the same paper.

This current paper is a more detailed and systematic study of the impact of crystal structure of Nb_2O_{5-x}, generated by pre-calcination, on the catalytic oxidation activity of supported MnO_x. It provides mechanistic insight into the structural interaction between Mn oxides and high temperature monoclinic Nb_2O_{5-x} for the catalytic oxidation of VOCs. All catalysts were characterized by BET, XRD, H_2-TPR and XPS, and the performance evaluated mainly in the catalytic oxidation of propane, chosen as model VOCs molecule. In addition, the results will be compared with the alumina-based catalysis using similar catalytic preparation and test conditions. The thermal stability of the optimized catalyst was also studied and substantiated.

2. Experimental

2.1. Catalyst preparation

Powdered Niobium hydrate ($Nb_2O_5 \cdot 5H_2O$) CBMM, San Paolo, Brazil) (BAFS) andγ-Alumina (Al_2O_3)(Sigma-Aldrich) were individually calcined in air from 500 °C to 1100 °C with a ramp rate of 3 °C /min to a the final temperature for 3 h. Upon cooling to room temperature various loadings of manganese nitrate hydrate ($Mn(NO_3)_2 \cdot 6H_2O$) (Sigma-Aldrich) were impregnated. The niobium hydrate calcined at 500, 700, 800, 900 and 1025 °C were given the notation of $Nb_2O_{5-x}@500$, $Nb_2O_{5-x}@700$, $Nb_2O_{5-x}@800$, $Nb_2O_{5-x}@900$ and $Nb_2O_{5-x}@1025$, respectively. The pre-calcined alumina was labelled $Al_2O_3@500$, $Al_2O_3@800$ and $Al_2O_3@1025$.

A set of catalysts synthesized using incipient wetness impregnation and designated, Z% MnO_x/ (1-Z%)Nb_2O_{5-x} (Y), where Z = 4, 6, 10, 20, 30 wt%, and Y = Nb_2O_{5-x} pre-calcined at 500 °C, 700 °C, 800 °C, 900 °C and 1025 °C. Each finished catalyst was dried in air at 110 °C overnight and heated to 400 °C at a rate of 2 °C/min and held at 400 °C in air for 3 h. Thermal Gravimetric Analysis (TGA) in air was used to establish 400 °C as adequate for complete decomposition of the nitrates. Similar methods and preparation conditions were used for the alumina-based catalysts, Z% MnO_x/ (1-Z%) Al_2O_3 (Y). Catalysts studied of greatest interest were, Fresh 20% MnO_x/Nb_2O_{5-x}(500) @400 °C, Fresh 20% MnO_x/Nb_2O_{5-x}(800)@400 °C, Fresh 20% MnO_x/Nb_2O_{5-x}(1025) @ 400 °C, Fresh 20% MnO_x/Al_2O_3(500)@400 °C, Fresh 20% MnO_x/Al_2O_3 (800)@400 °C, Fresh 20% MnO_x/Al_2O_3(1025)@400 °C, labelled as M-N500, M-N 800, M-N 900, M-N 1025, M-A500, M-A800 and M-A1025, respectively. Other loadings of MnO_x were also studied however, 20% appears to be optimum.

2.2. Catalysts characterization

Specific surface areas were determined using a Quantachrome ChemBET instrument and the single-point Bruauer-Emmett-Teller

(BET) method. All samples were degassed at 130 °C for over 2 h in nitrogen, at a flow rate of 30mn/min prior to measurements with the nitrogen adsorption isotherm generated at liquid nitrogen temperature 77 K (-196 °C).

X-ray powder diffraction (XRD) patterns were collected on a Rigaku diffractometer using Cu Ka radiation (λ = 0.15406 nm) at Voltage of 40 kV and current of 200 mA. Intensity data was recorded in 2θ range of 10-80°with scanning rate of 5°/min.

The thermal gravimetric analysis and differential scanning calorimetry (TG-DSC) profiles were recorded on a simultaneous thermal analyzer (NETZSCH STA 449 F3), with a heating rate of 10 °C /min under a continuous flow of air.

Raman measurements were performed on a Renishaw InVia Reflex micro-Raman spectrometer and recorded at room temperature in an imaging microscope with laser excitation at 514.5 nm in the backscattering light collection mode. The exciting wavelength of 514.5 nm from an Ar ion laser with a power of 10 mW was used for the catalysts.

Surface Oxidation states were investigated using X-ray photoelectron spectroscopy (XPS), conducted on a PHI5000 Versaprobe-II instruments using a Al-Ka monochromatic source. XPS spectra were recorded at room temperature and evacuated to below 10-7 Pa. The XPS were fitted to investigate the surface active species by measuring the binding energies, the spectral areas and the peak full width at half maxima using Multipak XPS software. All the spectra were calibrated with respect to the binding energy of C 1 s signal at 284.80 eV.

Temperature-programmed reduction (TPR) was performed using a Quantachrome instrument with 10% H_2 in argon at a total flow rate of 25 ml/min. The temperature range studied extended from room temperature to 900 °C at a heating rate of 10 °C /min.

2.3. Catalytic activity tests

Oxidation tests of propane were carried out in a fixed-bed quartz flow reactor (13 mm diameter) at ambient pressure with the total flow rate of 6.5 L h^{-1} and a gas hourly space velocity (GHSV) of 64800 h^{-1}. To avoid hot spots from the exothermic reaction and to improve flow distribution, about 0.1 ml of catalyst was diluted with 0.65 g fine quartz packed into the reactor and supported on quartz wool. The catalyst was pre-treated with flowing helium at 400 °C for about 2 h to clean the catalyst surface of volatile species such as absorbed H_2O and CO_2.

A cold trap was placed at the outlet of the reactor to condense water produced during the reaction prior to entering the gas chromatography (GC). Effluent gases of O_2, CO_2, C_3H_8 and N_2 were continuously analyzed by the micro GC (INFICON 3000 Micro GC equipped with 10 m Molsieve 5 A column, 8 m Plot U column). The GC was calibrated using 4 different certified standard gases before measurements were made. The temperature of the catalyst bed was measured with a K-type thermocouple inside the catalyst bed and controlled by an Omega CN7800 series temperature controller.

For propane oxidation, the final concentration of reactants was 0.1 vol % C_3H_8 + 17.85 vol % O_2 + balance N_2. The conversion vs temperature profiles were generated from 25 °C with steady state measurements taken in 25 °C increments up to 425 °C. For all tests, five steady state measurements were made to obtain five data points at each temperature. Carbon balances was calculated for each data point using nitrogen gas as an internal standard. Propane conversions were calculated as follows:

$$\text{Propane conversion (\%)} = \left(\frac{[C_3H_8]_{in} - [C_3H_8]_{out}}{[C_3H_8]_{in}} \right) \times 100$$

Isothermal aging tests were conducted in the process gas at 340 °C for about 30 h (90% conversion) for the best performing sample 20% MnO_x/Nb_2O_{5-x} (1025) @400 °C (M-N 1025). After aging the conversion vs temperature profile was again generated from a scan beginning at 25 °C to the final temperature.
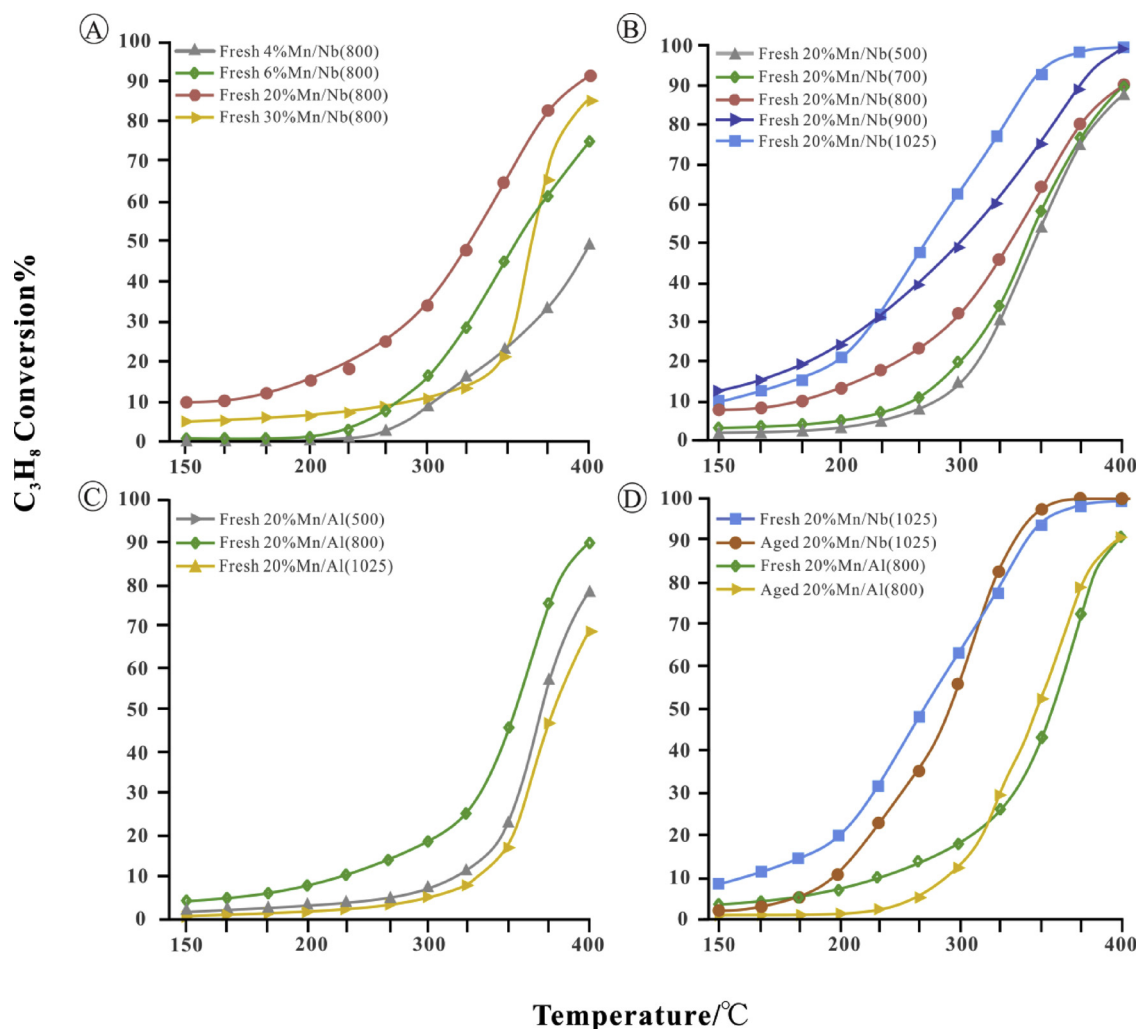
Fig. 1. Propane conversion versus temperature for various loadings of manganese (A), various pre-treated niobium oxide (B), various pre-treated alumina (C) and comparison of fresh and aged samples of M-N 1025 and M-A800 (D). Aging was conducted at 340 ∘C for 30 h with reaction gases flowing. Gas composition: C_3H_8 0.1 vol %; O_2 17.85 vol %, N_2 balance. Catalysis volume: 0.1 mL; GHSV: 64,800 (h^{-1}).

3. Results

3.1. Catalytic performance

The catalytic activity tests for propane were measured from 25 °C to 425 °C, at a GHSV of 64,800 (h^{-1}). Various loadings of MnO_x on Nb_2O_{5-x} with the latter pre-calcined at various temperatures were studied. The propane conversion vs. temperature plots for a series of MnO_x/Nb_2O_{5-x} and MnO_x/Al_2O_3 catalysts are presented in Fig. 1, and the reaction temperatures of T20, T50 and T90 (corresponding to propane conversion of 20%, 50% and 90%) are summarized in Table 1 for detailed comparison.

Fig. 1A indicates that Fresh 20% MnO_x/Nb_2O_{5-x} (800) @400 °C (M-N 800) performs best relative the other loadings. Fig. 1B shows that the highest activity is achieved with 20% MnO_x deposited on Nb_2O_{5-x} pre-calcined at 1025 °C (M-N 1025). Fig. 1C demonstrates that MnO_x over γ-Al_2O_3 pre-calcined at 800 °C generates the highest activity. Figs. 1D and 2, however, clearly shows that both fresh and aged 20%MnO_2/Nb_2O_{5-x} (1025) are more active and stable than 20% $MnO_x/γ$-Al_2O_3 (800 °C) also fresh and aged. Most surprising is the superiority of the 20% Mn catalysts deposited on pre-calcined Nb_2O_{5-x} (1025) relative to the Nb_2O_{5-x} calcined at lower temperatures. It was stated earlier that the Nb_2O_{5-x} (1025 °C) has a SSA < 5 m^2/g, considerably lower than Nb_2O_{5-x} (> 50 m^2/g) pre-calcined at lower temperatures. This indicates

a strong positive interaction between MnO_x and Nb_2O_{5-x} calcined at 1025 °C, independent of its low surface area. One may postulate that a defect structure has formed leading to enhanced activity, which will be discussed in the following section. Table 1 presents the temperature for 20, 50 and 90% conversion of propane.

To further explore the effect on the activation energy for oxidation
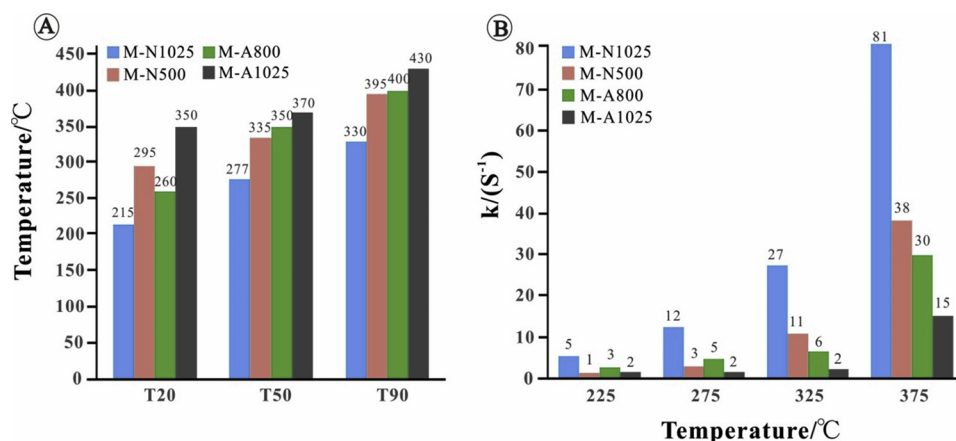
Table 1
Temperatures (°C) for % conversion of propane.

Catalyst	T20	T50	T90	Simplification
Fresh 4%Mn/Nb(800)@400 °C	335	400	–	
Fresh 6%Mn/Nb(800)@400 °C	310	350	–	
Fresh 30%Mn/Nb(800)@400 °C	355	370	425	
Fresh 20%Mn/Nb(500)@400 °C	295	335	410	M-N500
Fresh 20%Mn/Nb(700)@400 °C	265	330	400	M-N700
Fresh 20%Mn/Nb(800)@400 °C	265	337	395	M-N800
Fresh 20%Mn/Nb(900)@400 °C	198	300	375	M-N900
Fresh 20%Mn/Nb(1025)@400 °C	**215**	**275**	**340**	**M-N1025**
Fresh 20%Mn/Nb(1025)@500 °C	325	385	–	
Fresh 20%Mn/Nb(1025)@600 °C	365	450	–	
Fresh 20%Mn/Al(500)@400 °C	345	367	–	M-A500
Fresh 20%Mn/Al(800)@400 °C	300	356	400	M-A800
Fresh 20%Mn/Al(1025)@400 °C	350	370	–	M-A1025
Aged 20%Mn/Nb(1025)@400 °C	**230**	**285**	**335**	**AGEDM-N1025**
Aged 20%Mn/Al(800)@400 °C	314	345	395	AGEDM-A800

Fig. 2. Comparison of reaction temperature (A) and assumed first order in C_3H_8 reaction constants at T20 which is in the kinetic regime.

Table 2
Apparent Activation Energies for the oxidation of propane(kJ/mol).

	M-N1025	M-N500	M-A800	M-A1025
C_3H_8 Oxidation	39.52	76.04	69.80	121.40

of propane, the kinetic calculations are illustrated below. The assumed first order reaction rate constants of M-N 500, M-N 1025 M-A800 and M-A1025 at different temperatures were calculated (Fig. 2B) while the apparent activation energies (Ea) were also obtained (Table 2) based on the catalytic activity data. It should be stressed that, the operation was conducted at low conversions to ensure kinetic control: the GHSV and temperature was adjusted to maintain less than 20%–25% propane conversion. In addition, we also compare the conversion of propane oxidation by diluting 0.1 ml catalysis with quartz from 0.35 g to 0.75 g to ensure isothermal conditions. We have assumed first-order in C_3H_8 and pseudo-zero order in oxygen since it is present in a large excess of the pollutants. Rate constants were obtained from equations 1 and 2.

$$\ln\left(\frac{C_I}{C_O}\right) = kt = \frac{k}{GHSV} \tag{1}$$

$$r = -kC = \left(-A\exp\left(-\frac{E_a}{RT}\right)\right)C \tag{2}$$

where C_i is the inlet concentration and C_o is the outlet concentration of reactant and A is the pre-exponential factor.

The Arrhenius plots for C_3H_8 for Nb_2O_{5-x}-based and Al_2O_3-based samples are presented in Fig. 3. The results show that Nb_2O_{5-x}-based samples have relatively lower apparent activation energies and higher first order reaction rate constants compared to Al_2O_3-based samples for propane oxidation. M-N 1025 sample exhibits the highest reaction rate constant (k) from 225 °C to 375 °C and lowest apparent activation energy (Ea) from T20 to T50 for propane oxidation (39.52 kJ/mol) over the M-N 1025 sample.

3.2. Structural properties of catalysts

X-ray powder diffraction was used to study the evolution of the Nb_2O_{5-x} structure with various pre-calcination temperatures and the results are shown in Fig. 4. Patterns for bulk niobium oxide between 500 °C and 1025 °C show various reflections enabling the determination of different phases at each of these temperatures. Three phases of niobium oxide (i.e., pseudo-hexagonal, orthorhombic and monoclinic) are sequentially identified with the temperature increasing from 500 to 1025 °C (Fig. 4A). The pseudo-hexagonal Nb_2O_{5-x} phase is observed when the sample is calcined around 500 °C [31], and the orthorhombic structure is detected when the calcination temperature was increased to
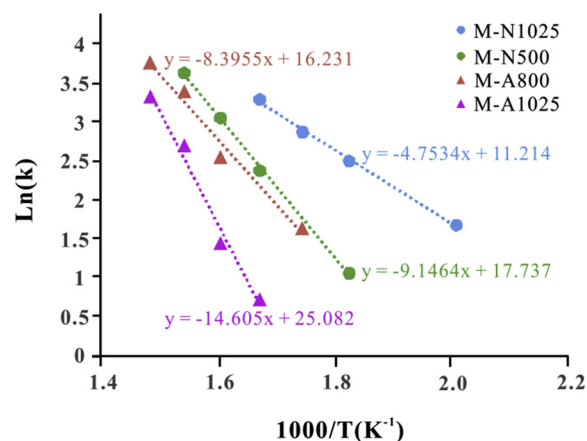

Fig. 3. Arrhenius plots for C_3H_8 oxidation under conditions of C_3H_8 0.1 vol %; O_2 17.85 vol %, N_2 balance with catalysis volume: 0.1 mL and GHSV: 64,800 (h^{-1}).

800 °C [31–35]. Further increasing the temperature to 900 °C very weak peaks corresponding to the monoclinic [33] are identified. For the sample obtained at 1025 °C, both the pseudo-hexagonal and orthorhombic phases change to monoclinic (c2/m and P2) Nb_2O_{5-x} [32–36].

Fig. 4B shows the manganese oxide supported on Nb_2O_{5-x} calcined at different temperatures, and the loading content of MnO_x is kept at 20 wt% for all samples. All samples show similar XRD patterns with the corresponding pure niobium oxide samples. In addition, there is no obvious shift of patterns for the mixed oxides compared with the pure Nb_2O_{5-x}, indicating that no Mn ions are incorporated into the Nb_2O_{5-x} lattice to form a solid solution. These phenomena are likely to suggest that the size of MnO_x and/or other potential Mn-O-Nb compounds are too small to be detected by XRD measurements.

In parallel, The BET results (Supplementary Fig. 1A) show that the surface area of Nb_2O_{5-x} decreases dramatically with increasing pre-calcination temperature due to the formation of new highly structured Nb_2O_{5-x} phases. The surface area of M-N 1025 sample is ~3.94 m²/g while Nb_2O_{5-x}@1025 is 2.13 m²/g and Nb_2O_5@500 is about 50 m²/g, Obviously, these are much lower than γ-Al_2O_3 and Al_2O_3-based samples (100 - 150 m²/g). Counterintuitively, sample M-N 1025 possesses the lowest surface area but highest catalytic propane activity among all samples evaluated.

Thermogravimetric mass loss (TG) and the associated endotherm of M-N 1025 was determined by the DSC heat flux (mW) between 0–1025 °C. The DSC-TG profile of M-N 1025 sample (Supplementary Fig. 1B) shows an initial endothermic weight loss around 100 °C −200 °C, corresponding to the loss of water. Low temperature niobium
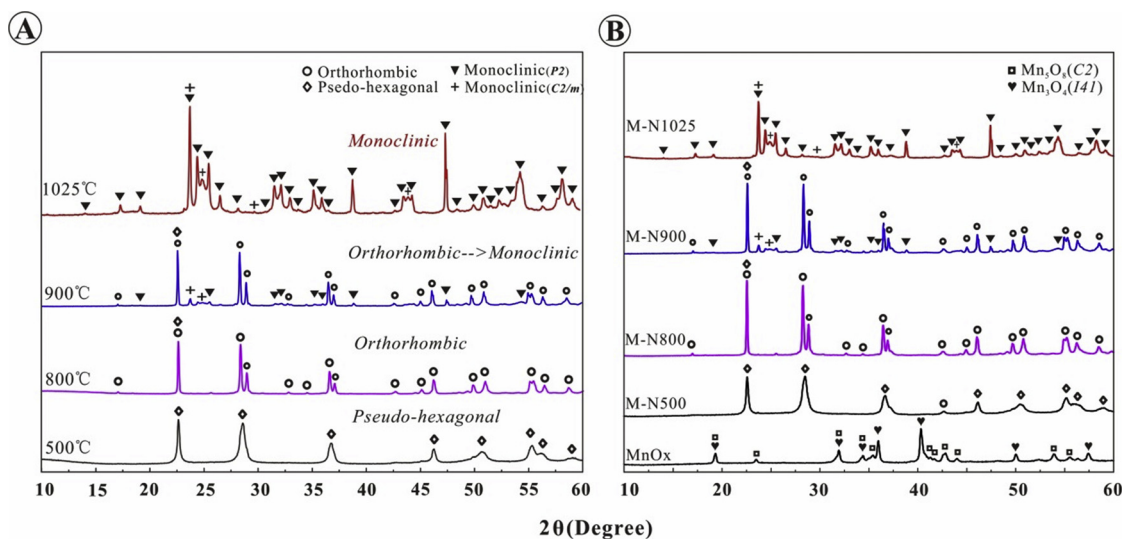
Fig. 4. The X-ray diffraction patterns of aged Nb_2O_{5-x} at different calcined temperatures (A) and 20%MnO_x on Nb_2O_{5-x} phases (B).

oxide is stable up to around 300 °C, after which little weight loss occurs with a slowly increasing DSC heat flux signal. A sharp endothermic peak occurs with a small weight loss (~1%) around 570 °C. which could be associated with the phase change of niobium oxide without a change of oxidation state. This seems to be confirmed by XRD pattern above 500 °C.

3.3. Surface properties and reducibility

3.3.1. Surface interaction

Raman spectroscopy provides a sensitive response to the detection of the bond order of metal oxides, especially in the region of metal-oxygen stretching modes. A higher metal oxygen bond order, corresponding to a shorter bond distance, shifts the Raman bond to higher wavenumbers [37]. In addition, metal oxides do not always occur in a crystalline form which may not be detected by XRD [38,39].

The Raman spectra of samples of interest are shown in Fig. 5 as a function of pre-calcination temperature. For niobium oxide (Fig. 5A) heated for 3 h at 500 °C, a broad, weak Raman band at ~900 cm^{-1} and a strong Raman band at ~688 cm^{-1} is observed. The Raman band of Nb_2O_{5-x} @500 °C in the low-wavenumber range around 240 cm^{-1} is weak. It should be noticed that the Raman bands below 200 cm^{-1} are due to lattice vibrations. The Raman features of Nb_2O_{5-x} @800 °C are similar to Nb_2O_{5-x} @500 °C except the intensity at ~688cm^{-1} and 200-300 cm^{-1} is stronger than Nb_2O_{5-x} @500 °C. It is very interesting that, for the Nb_2O_{5-x} sample treated at 900 °C for 3 h, the results indicate that a new phase of Nb_2O_{5-x} sample is initiated and a new small band at ~992 cm^{-1} is present. Instead of the previous Raman bands at ~688 cm^{-1}, sample Nb_2O_{5-x} @900 °C possesses twin peaks of the Raman spectra at ~647cm^{-1} and ~685 cm^{-1}. For the Nb_2O_{5-x} @ 1025 °C sample, the crystal phase transformation is detected by the bands at 992cm^{-1} and the twin peak at ~626 cm^{-1} and ~677 cm^{-1}, both of them are much sharper and more intense than that of Nb_2O_{5-x} @ 900 °C. This new phase is also confirmed by XRD and identified as the monoclinic phase (Fig. 4). Furthermore, the bands at ~903 cm^{-1} and 260 cm^{-1} (shift from 240 cm^{-1}) are more resolved than all samples calcined below 1025 °C. It has been reported that the Raman band at ~930 cm^{-1} refers to a highly distorted octahedral structure of NbO_6, and the strong and twin peaks around ~ 650 cm^{-1} assigned to the symmetric stretching mode of the niobia polyhedra [38,39]. The broad
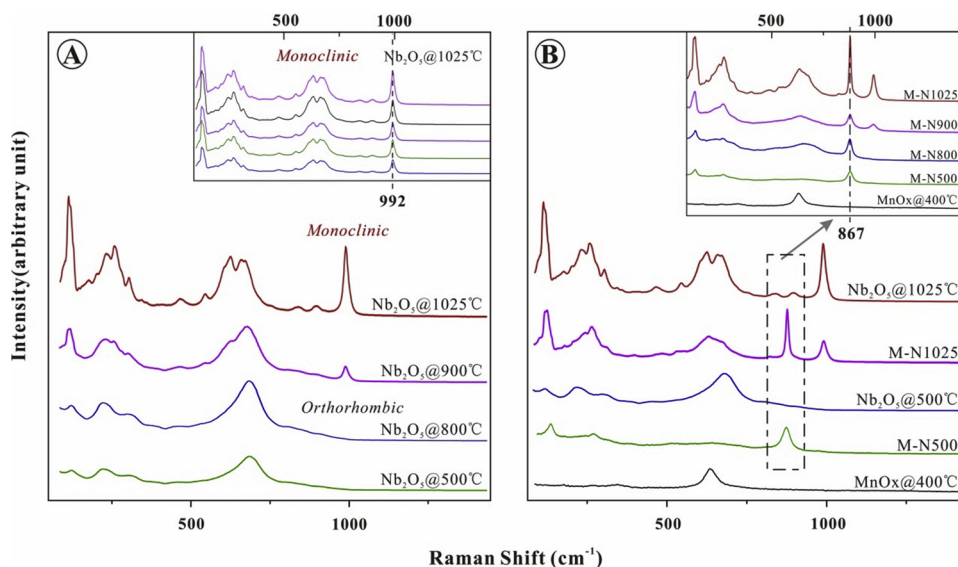

Fig. 5. Raman spectra of bulk Nb_2O_{5-x} at various pre-calcination temperature (A) and.
(B) Mn- Nb_2O_{5-x} -based catalysts at various temperature.

band at ~688 cm^{-1} of Nb$_2$O$_{5-x}$ @500 °C is characteristic of the vibrations of Nb-O-Nb bridges from slightly distorted octahedral NbO$_6$ connected with shared corners. The band between 150 cm^{-1} and 300 cm^{-1} is assigned to the bending modes of Nb-O-Nb linkages. The doublet Raman band at ~626 cm^{-1} and ~677 cm^{-1} of Nb$_2$O$_{5-x}$ @1025 °C, which shifts from ~688 cm^{-1} for low temperature niobium oxide, associated with vibrations of Nb–O–Nb bridges, suggests that the structures of the niobium oxide species are dependent on the relative pre-calcination temperature [38–40].

Fig. 5B displays the Raman results after 20%MnO$_x$ was deposited and a sample of pure manganese oxide calcined at 400 °C (MnO$_x$@ 400 °C). All Nb$_2$O$_{5-x}$ -based catalysts(M-N 500, M-N 800, M-N 900, M-N 1025) show a new band at ~867 cm^{-1}, which is not observed for pure manganese and/or pure niobium oxide. In contrast, among all Al$_2$O$_3$-based samples, only a Raman band of manganese oxide at ~636 cm^{-1} is observed (Supplementary Fig. 2). Therefore, it is reasonable to deduce that there is an interaction between the oxides of manganese and niobium oxide which may form a unique compound. Secondly, manganese oxide calcined at 400 °C possesses a Raman band at ~636cm^{-1}, which is incorporated into the twin peak and then forms a strong and broad Raman spectra ~636 cm^{-1} with the M-N 1025 sample, whereas in M-N 500, the counterpart of Raman band is not observed. Thirdly, Raman studies reveal that the new compound containing oxides of manganese and niobium possesses a similar structure to that of H-Nb$_2$O$_5$ (Nb$_2$O$_{5-x}$ @1025 °C) (Fig. 5B) since apart from the new peaks (~867 cm^{-1}) of the spectra, M-N 1025 maintains the characteristic bands of Nb$_2$O$_{5-x}$ @1025 °C at ~992cm^{-1} and 260 cm^{-1} without shifting.

3.3.2. Surface oxidation states and defect sites

To further confirm the surface composition and chemical state of the atoms in Nb$_2$O$_{5-x}$-based samples, X-ray photoelectron spectroscopy (XPS) was conducted with results shown in Fig. 6. The reference binding energy for Nb^{5+} 3d$_{5/2}$, Nb^{4+} 3d$_{5/2}$ and Nb^{2+}3d$_{5/2}$ core levels are listed in the Supplementary Table 1 [41–46]. The quantitative analysis of relative content of different ions (e.g., Nb^{5+}, Nb^{4+}, Mn^{4+} and Mn^{3+}) on the surface is obtained by calculating the area ratios of corresponding species derived from the raw XPS data, as shown in Table 3.

Fig. 6A shows the evolution of the Nb3d doublet with increasing pre-calcination temperature of the Nb$_2$O$_{5-x}$ only. The doublet seen in the Nb 3d spectra constitutes peaks of Nb3d$_{5/2}$ and Nb 3d$_{3/2}$ with the oxide states of Nb analyzed by fitting the curves of the Nb 3d$_{5/2}$ XPS bands. The entire position of Nb 3d$_{5/2}$ deconvoluted experimental XPS bands (Fig. 6A) indicate Nb^{5+} (207.17 eV – 207.52 eV) and Nb^{4+} (205.38 eV – 206.81 eV) oxidation state, which consistent with the binding energies in the literature [41–48]. More specifically, the Nb 3d doublet of the original data of XPS occur at lower binding energies with increasing pre-calcination temperature of the niobium oxide (from M-N 500 to M-N 1025). This is likely due to a change in chemical environment of the niobium atoms by lattice deformation induced a stronger deformation niobium oxide when calcined at higher temperature. Accordingly, it is found that with the loading of 20% MnO$_x$, the average ratios of Nb^{4+}/ Nb^{5+} increases in the order of M-N 500 < M-N 800 < M-N 900 < M-N 1025 (Table 3). The highest ratio of Nb^{4+}/ Nb^{5+} in this study is 0.92 for sample M-N 1025. In other words, the Nb$_2$O$_{5-x}$ pre-calcined at 1025 °C has a composition of Nb$_2$O$_{5-x}$ where 0 < x < 1, which indicates oxygen loss from the surface. In addition, the experimental Nb 3d$_{5/2}$ could also be deconvoluted into the two contributions of Nb^{4+} and Nb^{5+} with a Nb^{4+}/ Nb^{5+} ratio of 0.51 in the sample of pure niobium oxide calcined at 1025℃. The peak of Nb^{5+} is the only component analyzed by XPS in the sample of pure Nb$_2$O$_{5-x}$ @ 500 °C. The highest ratio of Nb^{4+}/ Nb^{5+} achieved in the niobium pre-calcined at 1025 °C indicates that the pre-calcination temperature of niobium oxide plays an important role in the oxidation state and thus catalytic activity.

The O 1 s spectra of M-N 500, M-N 800, M-N 900 and M-N 1025 are

shown in Fig. 6B depends on both the chemisorbed oxygen species (Oα) and the lattice oxygen (Oβ). It should be noted that the peak for adsorbed oxygen is generally weaker than that of lattice oxygen and could be an indicator of oxygen vacancies [47–49]. As a whole, the peak at 529.40–529.84 eV corresponds to O$_β$, whereas the experimental bands at 530.89–532.00 eV can be ascribed to surface-absorbed oxygen species (O$_α$, i.e. O$_2$$^{2-}$, O$^-$, OH$^-$ or CO$_3$$^{2-}$) [16,50,51]. The O 1 s spectra could be deconvoluted into two contributions, surface oxygen and lattice oxygen, whereas the M-N 1025 sample could be fitted with three peaks at 532.00 eV, 530.89 eV and 529.40 eV. The former two could be assigned to surface oxygen with various adsorbed oxygen species, and the latter attributed to the lattice oxygen. It is generally accepted that the surface adsorbed oxygen (Oα) possesses greater mobility than lattice oxygen and may give rise to beneficial spillover phenomena at the solid surface [16,19]. As illustrated in Table 3, the highest O$_α$/O$_β$ ratio is attained for sample M-N 1025 (O$_α$/O$_β$ = 1.47), confirming the high proportion of oxygen vacancies present. In associated with the XPS data, obtained for pure niobium oxide calcined at different temperatures, shows an increasing O$_α$/O$_β$ ratio as follows: M-N 500 ≈Nb$_2$O$_{5-x}$ @ 500 < M-N 800 < M-N 900 < Nb$_2$O$_{5-x}$ @1025 < M-N 1025 (Table 3), which again indicates the effect of pre-calcined niobium on the presence defect structures. This result is consistent with Nb 3d.

Fig. 6C shows the Mn 2p XPS spectra of samples in a range between 635 eV and 662 eV. The binding energies at 640.00–650.00 eV and 650.00–660.00 eV can be attributed to Mn 2p$_{3/2}$ and Mn 2p $_{2/1}$, respectively [43,52]. The deconvoluted Mn 2p spectra for all samples could be assigned to three contributions, the lowest binding energy being ascribed to Mn^{2+} at ~640.98 eV – 641.68 eV. The range of 642.06 eV to 643.19 eV could be assigned to Mn^{3+}. Mn^{4+} has the highest binding energy and can be assigned range of 644.64–645.02 eV. These results are in agreement with the literature [43,52–55]. Table 3 lists the relative surface composition of manganese with different valences. The highest Mn^{3+}/Mn^{2+} and Mn^{3+}/Mn^T ratio obtained is from M-N 1025, whereas the lowest ratios occur for M-N 500 (Table 3). It is possible that the increasing component of the Mn^{3+}&Mn^{4+} pair is associated with the active catalytic states. It is possible that the niobium oxide calcined above 1000 °C has high interaction with manganese oxide and consequently induces an increasing proportion of active phases of manganese on the surface of catalyst. This tentative conclusion is in fair agreement with the Raman band at 867cm^{-1} (Fig. 5).

3.3.3. Reducibility

H$_2$-TPR was conducted to test the reducibility of samples. According to the literature [56,57], the reduction of manganese oxides can be described by the following steps: MnO$_2$ → Mn$_2$O$_3$ → Mn$_3$O$_4$ → MnO. However, the TPR profiles could also depend on the Mn cations located in different environments [58].

Fig. 7 shows the H$_2$-TPR profiles of the fresh manganese oxide catalysts supported on different Nb$_2$O$_{5-x}$ and Al$_2$O$_3$ carriers as the function of reduction temperature (°C). In M-N 1025 the most active catalyst, three peaks are observed whereas only two peaks are observed in the other samples. The two peaks at 282 °C and 307 °C could be ascribed to the reduction of MnO$_2$ (MnO$_2$ to Mn$_2$O$_3$) and the reduction of Mn$_2$O$_3$ (Mn$_2$O$_3$ to Mn$_3$O$_4$), respectively. The last broad peak at 385 °C could be attributed to the reduction of Mn$_3$O$_4$ (Mn$_3$O$_4$ to MnO). In contrast only two peaks are observed in the TPR profile for all the other samples. In the case of M-N 900, M-N 800, M-N 500 and M-A800, the two peaks could be attributed to the reduction of Mn$_2$O$_3$(Mn$_2$O$_3$ to Mn$_3$O$_4$) and Mn$_3$O$_4$ (Mn$_3$O$_4$ to MnO), respectively. The lowest reduction temperature (305 °C) for Mn$_2$O$_3$ was obtained by M-N 900, whereas 345 °C was obtained for M-N 800. Furthermore, the reduction temperature of Mn$_2$O$_3$ follows the order of M-N 1025 < M-N 900 < M-N 800 < M-N 500 ≈ M-A800. It is reasonable to conclude that the M-N 1025 sample has the highest reducibility which generates higher catalytic oxidation activity when interacting with the manganese species. The reduction of MnO$_2$ is only observed in M-N 1025 at 282 °C which
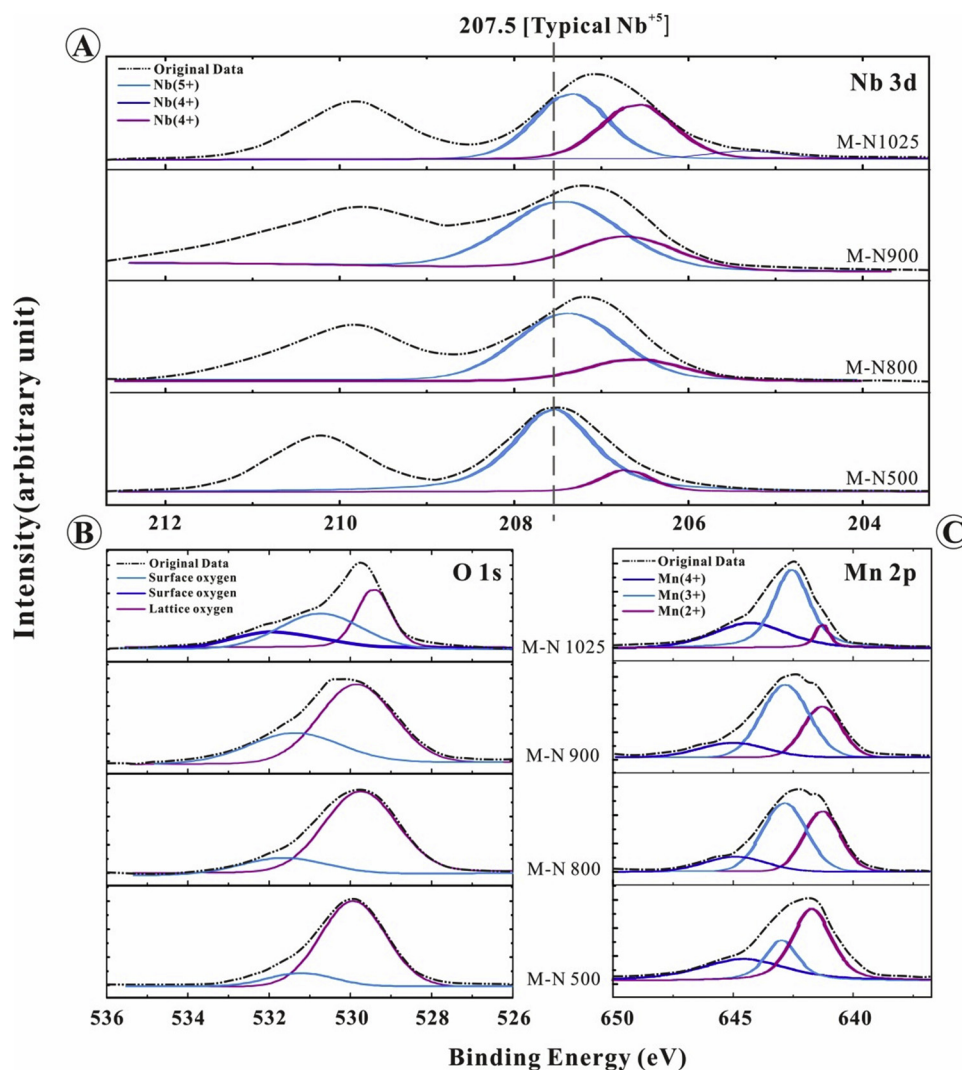
Fig. 6. Nb 3d (A), O 1 s (B) and Mn 2p$_{3/2}$(C) XPS spectra of Nb$_2$O$_{5-x}$ -based samples.

likely correlates with the relative larger amounts of Mn^{4+} on the surface. Negligible amounts of Mn^{4+} species are present on the surface of low temperature calcined niobium oxide and γ-alumina. Another possibility for the peak of MnO$_2$ reduction could be the synergistic effect between Mn and Nb on sample M-N 1025, which enhances the redox properties of Mn$_{4+}$/Mn$_{3+}$ pair while not for the others.

4. Discussion

For propane oxidation on niobium-based catalysts, a number of parameters, such as catalyst crystallite size, surface area, reducibility of the manganese species, and manganese content are believed to impact catalytic performance [57–60]. Generally, BET surface area and the concentration of manganese are usually important factors in determining catalytic activity. This is clearly not the case of for niobium oxide as a carrier material for MnO$_x$. Certainly our data indicates that the catalytic activity of MnO$_x$/ Nb$_2$O$_{5-x}$ increases with manganese loading up to 20%, but performance declines at a 30% loading (Fig. 1A). The data for MnO$_x$ on Nb$_2$O$_{5-x}$ (1025 °C) is consistent with our previous observations on Co/NbO$_x$ which also shows an increased activity for pre-calcined Nb$_2$O$_{5-x}$ [30] independent of BET surface area. For example, the surface area increases in the order of M-N 1025

Table 3
XPS results of the Mn2p$_{3/2}$, Nb3d$_{5/2}$ and O 1 s for Nb$_2$O$_{5-x}$ -based catalysts.

Catalysts	Relative Surface Content								Surface Atom Ration
	Mn 2p$_{3/2}$			Nb 3d$_{5/2}$		O 1 s			
	Mn^{3+}/Mn^{2+}	Mn^{3+}/Mn^{4+}	Mn^{3+}/Mn^T	Nb^{4+}/Nb^{5+}	Nb^{4+}/Nb^T	O$_\alpha$ (%)	O$_\beta$ (%)	O$_\alpha$/O$_\beta$	Mn/Nb/O
M-N1025	9.29	1.89	0.61	0.92	0.48	59.39	43.41	1.47	28/4/68
M-N900	1.8	3.58	0.54	0.41	0.29	29.7	70.3	0.42	16/13/71
M-N800	1.36	2.83	0.48	0.15	0.13	19.5	80.5	0.24	16/14/70
M-N500	0.51	0.70	0.23	0.13	0.11	12.88	87.12	0.15	10/20/70

*Mn^T = (Mn^{2+} + Mn^{3+} + Mn^{4+}); Nb^T = (Nb^{4+} + Nb^{5+}).
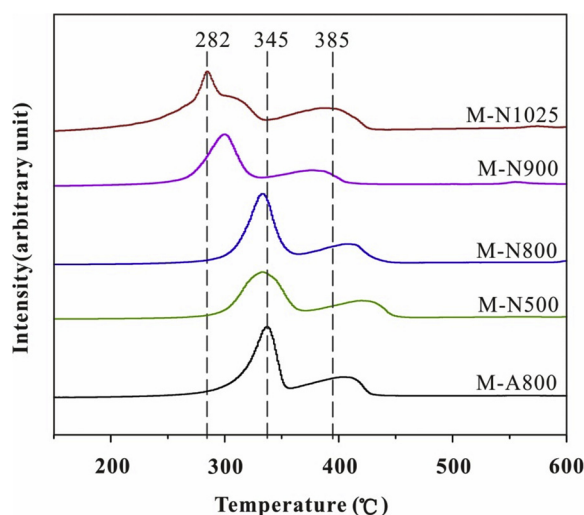
Fig. 7. H$_2$-TPR profiles of the MnO$_x$- Nb$_2$O$_{5-x}$ -based and Al$_2$O$_3$-based samples.

(2.13 m^2/g) < M-N 900 < M-N 800 < M-N 500 (~50 m^2/g), whereas the catalytic performance shows the opposite trend. Although the catalytic performance increases with increasing the pre-calcination temperatures of Nb$_2$O$_5$, the most dramatic increase occurs above 1000 °C which is related to a phase transition to monoclinic. The catalytic performance coupled with characterization data lead us to conclude the phase change effect of Nb$_2$O$_{5-x}$ @1025 °C on improving the catalytic properties with the following two possible reasons: (1) the presence of oxygen vacancies and (2) the proper Mn^{3+}/Mn^{4+} ratios induced by the interaction between Nb$_2$O$_{5-x}$ @1025 °C and MnO$_x$.

4.1. Effect of pre-calcination temperature on the structure of Nb$_2$O$_5$

The increasing pre-calcination temperature of niobium oxide leads to phase transformations and a mixture of monoclinic phases of Nb$_2$O$_{5-x}$ containing non-stoichiometric oxides (Nb$_{12}$O$_{29}$) formed around 1025 °C. This generates an abundance of oxygen vacancies, beneficial to propane oxidation.

Consistent with characterization results in the literatures [31–35,61], it is reasonable to propose the structure evolution of niobium oxide with increasing calcination temperature follows the schematic diagram Fig. 8. Below or around 500 °C, niobium oxide remains amorphous but then changes to a pseudo-hexagonal structure (TT-Nb$_2$O$_5$) [31,35]. Orthorhombic crystal (T-Nb$_2$O$_5$) could be obtained at temperatures of 600 - 800 °C [31,34–36]. One of the monoclinic phases initially formed above 900 °C and then achieves the mixture of monoclinic Nb$_2$O$_5$ and monoclinic Nb$_{12}$O$_{29}$ around 1025 °C where stoichiometric Nb$_2$O$_5$ converts to a higher proportion of non-stoichiometric niobium oxide, generating oxygen vacant sites [32].

The XRD results (Fig. 4) of M-N 1025 sample and Nb$_2$O$_{5-x}$ @1025 °C sample exhibit a mixture of monoclinic phases with spatial group of P$_2$ and C$_2$/m, which contain non-stoichiometric monoclinic niobium oxides, Nb$_{12}$O$_{29}$. This is consistent with the Raman structure (Fig. 5) of M-N 1025 which possesses the highly distorted cell of NbO$_6$ octahedra, where the cells are linked by edge-sharing. The non-stoichiometric niobium oxides formed due to the crystallographic shearing of highly distorted octahedral cells of NbO$_6$ unit above 1000 °C where the niobium oxide octahedral changes its linkage from corner to edge-sharing and possess the Nb atoms displaced from the center of the NbO$_6$ cell [32,62–64]. This kind of shearing plane and the modified linkage type of NbO$_6$ blocks facilitate the formation of monoclinic niobium with non- stoichiometric component, which in turn allow the niobium ion coordination to accommodate large oxygen deficiencies [62,64]. Marucco [65] previously observed Nb$_{12}$O$_{29}$ stable at temperature between 1000 °C and 1100 °C, later, Kikuchi et al. [66] and Iijima et al. [67,68] confirmed oxygen vacancies using high resolution electronic microscopy which displayed complex point defects in f Nb$_{12}$O$_{29}$. In addition, Janninck et al. [69] and Marucco [70] reported the oxygen vacancies in monoclinic niobium oxide with stoichiometry deviations by measuring the electrical conductivity as a function of oxygen partial pressure.

4.2. Effect of Nb$_2$O$_{5-x}$ structure on the interaction between niobium and manganese

A set of MnO$_x$/Nb$_2$O$_{5-x}$ catalysts were prepared by an incipient wetness impregnation and with niobium oxide pre-calcined from 500 °C to 1100 °C. The catalytic properties were evaluated by the total oxidation of propane. It was reported that hydrocarbon oxidation (i.e. propane) over manganese oxides occurs through a Mars-Van Krevenlen (M-K) mechanism involving the participation of lattice oxygen by a redox cycle [58–60,71,72]. The presence of higher surface oxygen species and oxygen vacancies in sample M-N 1025 provides relatively high freedom for the movement of lattice oxygen. Owing to the enrichment of oxygen vacancies, the absorbed oxygen could reduce the surface Gibbs energy and form surface active oxygen species, which could ultimately promote oxygen reactivity and propane activation in oxidation reactions [73]. In association with the effect of abundant
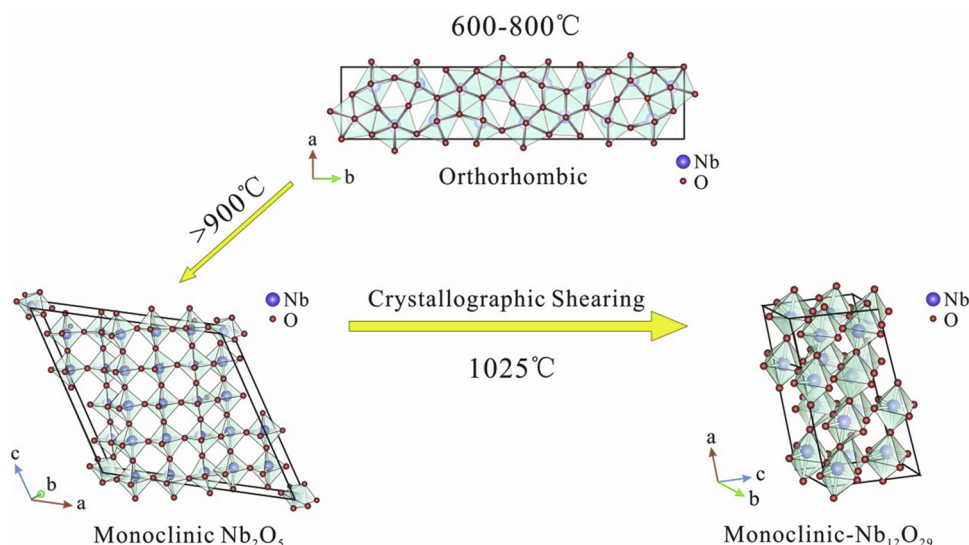

Fig. 8. Structure evolution of niobium oxide calcinated at different temperatures (Modified after [31–35]).
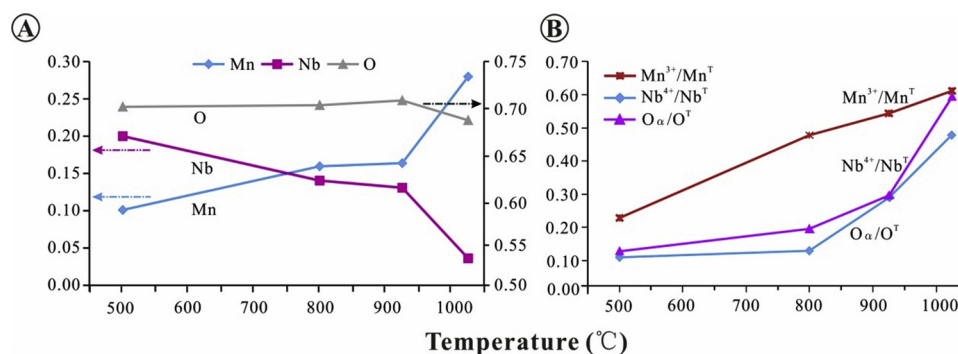
Fig. 9. Relative ratio of surface atom (A) and surface valence content (B) as a function of MnO_x supported by Nb_2O_{5-x} obtained at different temperatures.

oxygen vacancies, the enhanced redox properties of the surface Mn^{3+}/Mn^{4+} pair raised by the interaction between manganese and active niobium oxide contribute to the decreasing of apparent activation energy for this reaction. In fair agreement with this mechanism, a relatively low apparent activation energy for propane oxidation obtained in M-N 1025 (39.52 kJ/mol) of this study.

The surface composition and valence states of metal ions were further analyzed. Based on the aforementioned results and the literature, a stronger interaction between Nb_2O_{5-x} @1025 °C and MnO_x leads to high surface Mn^{3+} and the proper ratio of Mn^{3+}&Mn^{4+} which are the active promoters for the total oxidation of propane.

The Raman results demonstrated that (Fig. 6) as the pre-calcinating temperature of niobium species increases, the new peak of Nb_2O_{5-x} based samples become sharper and more intense at 867 cm^{-1} and the twin peak of manganese oxide at ~636 cm^{-1} becomes much stronger and broader accordingly. The new peak around 867 cm^{-1} observed in Raman spectra associated with XPS analysis (Fig. 9) indicate the corresponding dependence of the pre-calcination temperature on the surface concentration of manganese, niobium and oxygen. As the pre-calcination temperature of niobium oxide increases from 500°C to 1025°C, the relative content of surface manganese increases from 10% to 28% while niobium decreases from 20% to 4% (Fig. 9A). This phenomenon could be ascribed to the interaction of manganese species with Nb_2O_{5-x}@1025, in which the unique structure of higher temperature niobium oxide is capable to induce enrichment of surface-active manganese species. Fig. 9B exhibits that, among all species on the catalyst surface, the remarkably increasing ratio of Mn^{3+}/(Mn^{2+} + Mn^{3+} + Mn^{4+}) occurs with increasing pre-calcination temperature revealing the distinct effect of niobium oxide phases on the surface valence states of the manganese species. It should be stressed that the Nb^{4+}/Nb^{5+} ratio increases with the increase of Nb^{4+} due not only to the phase change of niobium oxide itself, but also the interaction with the surface manganese species. Additionally, the comparably high content of Mn^{4+} present on Nb_2O_{5-x} @1025 °C is further substantiated by H_2-TPR profile (Fig. 7), in which the reduction of MnO_2 (MnO_2 to Mn_2O_3) exclusively observed in M-N 1025. Apart from the strong interaction between high temperature niobium oxide and manganese oxide, those results demonstrate the active catalytic component is the Mn^{3+}&Mn^{4+} couple as well. In addition to the proper content of Mn^{3+}&Mn^{4+}, the interaction between manganese and niobium species are capable to further enhance the oxygen vacancy of the material [74]. The increased oxygen vacancies formed in the Mn-O-Nb material in turn increase the mobility of oxygen in the lattice of manganese, which ultimately enhances the catalytic oxidation properties. It is fair agreement with the literature that Mn_3O_4 with the surface partially reduced species possesses a high concentration of oxygen vacancies and higher catalytic activity for hydrocarbon oxidation rather than a surface with a similar stoichiometry manganese oxide [17,18].

The generally consistent results obtained from Raman, XPS and TPR in association with the literature demonstrate the stronger interaction

occurs between Nb_2O_{5-x} @1025 °C and MnO_x, providing the proper ratio of Mn^{3+} & Mn^{4+} and high oxygen mobility on the catalyst surface. Therefore, it is reasonable to propose that a new Mn-O-Nb specie with a large amount of active manganese is formed in the M-N 1025 sample, which could largely enhance the catalytic activity for propane oxidation by achieving the synergistic catalytic effect between MnO_x and Nb_2O_{5-x} @1025 °C.

5. Conclusion

Manganese oxides supported on niobium oxide have been extensively characterized and evaluated for total oxidation of propane. Niobium oxide pre-calcined above 1000 °C forms a specific monoclinic phase giving the sample M-N 1025 high performance for propane oxidation, regardless of very low specific BET surface area (3.94 m^2/g). The distinctive catalytic performance is further shown with an activation energy of 39.52 kJ/mol for propane combustion, which is much lower that for the M-N 500 sample (76.04 kJ/mol for propane combustion.

XRD, Raman and XPS have been used to identify the presence of an abundance of oxygen vacancies in monoclinic- Nb_2O_{5-x} with a high ratio of Nb^{4+}/Nb^{5+} coupled with the Mn^{3+}/Mn^T ratio induced by the strong interaction between the two. These results agree with the enhanced performance of C_3H_8 combustion. A high ratio of Nb^{4+}/Nb^{5+} appears to be the most significant surface composition in its promoting effect on MnO_x. The excellent catalytic performance reveals that the phase transformation of niobium oxide above 1000 °C is one of the most important factors that influences the catalytic activity. Additionally, the distinctive catalyst-carrier interaction between manganese and monoclinic- Nb_2O_{5-x} achieves and enhances the synergistic catalytic effect.

Appendix A. Supplementary data

Supplementary material related to this article can be found, in the online version, at doi:https://doi.org/10.1016/j.apcatb.2018.11.066.

References

[1] N. Li, F. Gaillard, Catalytic combustion of toluene over electrochemically promoted Ag catalyst, Appl. Catal. B Environ. 88 (2009) 152–159.

[2] P. Papaefthimiou, T. Ioannides, X.E. Verykios, Performance of doped Pt/TiO$_2$ (W^{6+}) catalysts for combustion of volatile organic compounds (VOCs), Appl. Catal. B Environ. 15 (1998) 75–92.

[3] F.N. Aguero, B.P. Barbero, L. Gambaro, L.E. Cadús, Catalytic combustion of volatile organic compounds in binary mixtures over MnO$_x$/Al$_2$O$_3$ catalyst, Appl. Catal. B Environ. 91 (2009) 108–112.

[4] A.R. Gandhe, J.S. Rebello, J.L. Figueiredo, J.B. Fernandes, Manganese oxide OMS-2 as an effective catalyst for total oxidation of ethyl acetate, Appl. Catal. B Environ.

72 (2007) 129–135.

[5] R.M. Heck, R.J. Farrauto, S.T. Gulati, Catalytic Air Pollution Control, third edition, (2012).

[6] K. Everaert, J. Baeyens, Catalytic combustion of volatile organic compounds, J. Hazard. Mater. 109 (2004) 113–139.

[7] J.J. Spivey, J.B. Butt, Literature Review: deactivation of catalysts in the oxidation of volatile organic compounds, Catal. Today 11 (1992) 465–500.

[8] L. Van De Beld, M.C. Van Der Ven, K.R. Westerterp, A kinetic study of the complete oxidation of ethene, propane and their mixtures on a Pd/Al₂O₃ catalyst, Chem. Eng. Process. Process Intensif. 34 (1995) 469–478.

[9] F. Diehl, J.B. Jr, D. Duprez, I. Guibard, G. Mabilon, Catalytic oxidation of heavy hydrocarbons over Pt/Al₂O₃. Influence of the structure of the molecule on its reactivity, Appl. Catal. B Environ. 95 (2010) 217–227.

[10] G. Salek, P. Alphonse, P. Dufour, S. Guillemet-Fritsch, C. Tenailleau, Low-temperature carbon monoxide and propane total oxidation by nanocrystalline cobalt oxides, Appl. Catal. B Environ. 147 (2014) 1–7.

[11] V.H. Vu, J. Belkouch, A. Ould-Dris, B. Taouk, Catalytic oxidation of volatile organic compounds on manganese and copper oxides supported on titania, AIChE J. 54 (2010) 1585–1591.

[12] M. Baldi, V.S. Escribano, J.M.G. Amores, F. Milella, G. Busca, Characterization of manganese and iron oxides as combustion catalysts for propane and propene, Appl. Catal. B Environ. 17 (1998) L175–L182.

[13] C.K. Sang, G.S. Wang, Catalytic combustion of VOCs over a series of manganese oxide catalysts, Appl. Catal. B Environ. 98 (2010) 180–185.

[14] R. Spinicci, M. Faticanti, P. Marini, S. De Rossi, P. Porta, Catalytic activity of LaMnO₃ and LaCoO₃ perovskites towards VOCs, J. Mol. Catal. A Chem. 197 (2003) 147–155.

[15] W. Si, Y. Wang, S. Zhao, F. Hu, J. Li, A facile method for in situ preparation of the MnO₂/LaMnO₃ catalyst for the removal of toluene, Environ. Sci. Technol. 50 (2016) 4572–4578.

[16] M. Piumetti, D. Fino, N. Russo, Mesoporous manganese oxides prepared by solution combustion synthesis as catalysts for the total oxidation of VOCs, Appl. Catal. B Environ. 163 (2015) 277–287.

[17] B. Bai, J. Li, J. Hao, 1D-MnO₂, 2D-MnO₂ and 3D-MnO₂ for low-temperature oxidation of ethanol, Appl. Catal. B Environ. 164 (2015) 241–250.

[18] K. Ramesh, L. Chen, F. Chen, Y. Liu, Z. Wang, Y.F. Han, Re-investigating the CO oxidation mechanism over unsupported MnO, Mn₂O₃ and MnO₂ catalysts, Catal. Today 131 (2008) 477–482.

[19] J. Wang, J. Li, C. Jiang, P. Zhou, P. Zhang, J. Yu, The effect of manganese vacancy in birnessite-type MnO₂ on room-temperature oxidation of formaldehyde in air, Appl. Catal. B Environ. 204 (2017) 147–155.

[20] A. Simson, K. Roark, R. Farrauto, A feasibility study of niobium-containing materials for nitrogen storage in three way catalytic converters, Appl. Catal. B Environ. 158–159 (2014) 106–111.

[21] T.S. Mozer, F.B. Passos, Selective CO oxidation on Cu promoted Pt/Al₂O₃ and Pt/Nb₂O₅ catalysts, Int. J. Hydrogen Energy 36 (2011) 13369–13378.

[22] F.B. Noronha, M. Schmal, M. Primet, R. Fréty, Characterization of palladium-copper bimetallic catalysts supported on silica and niobia, Appl. Catal. 78 (1991) 125–139.

[23] D.A.G. Aranda, F.B. Passos, F.B. Noronha, M. Schmal, Activity and selectivity of Pt-Sn/ Nb₂O₅ in n-heptane conversion, Catal. Today 16 (1993) 397–405.

[24] T. Uchijima, SMSI effect in some reducible oxides including niobia, Catal. Today 28 (1996) 105–117.

[25] J.-M. Jehng, I.E. Wachs, The molecular structures and reactivity of supported niobium oxide catalysts, Catal. Today 8 (1990) 37–55.

[26] D.A.G. Aranda, M. Schmal, Ligand and geometric effects on Pt/ Nb₂O₅ and Pt–Sn/ Nb₂O₅ catalysts, J. Catal. 171 (1997) 398–405.

[27] S.M. Maurer, D. Ng, E.I. Ko, Structural and acidic properties of aerogels of niobia, niobia/selica, and niobiattania, Catal. Today 16 (1993) 319–331.

[28] X. Gao, I.E. Wachs, M.S. Wong, J.Y. Ying, Structural and Reactivity Properties of Nb☐MCM-41: comparison with That of Highly Dispersed Nb₂O₅ /SiO₂ Catalysts, J. Catal. 203 (2001) 18–24.

[29] S.M. Maurer, E.I. Ko, Synthesis and characterization of niobia-containing aerogels, Catal. Lett. 12 (1992) 231–237.

[30] W. Xiang, X. Han, J. Astorsdotter, R. Farrauto, Catalysts promoted with niobium oxide for air pollution abatement, Catalysts 7 (2017) 144.

[31] I. Nowak, M. Ziolek, Niobium compounds: preparation, characterization, and application in heterogeneous catalysis, Chem. Rev. 99 (1999) 3603–3624.

[32] C. Nico, T. Monteiro, M.P.F. Graça, Niobium oxides and niobates physical properties: Review and prospects, Prog. Mater. Sci. 80 (2016) 1–37.

[33] L. Mestres, M.L. Martínez-Sarrión, O. Castaño, J. Fernández-Urbán, Phase diagram at low temperature of the system ZrO₂/Nb₂O₅, Zeitschrift Für Anorg. Und Allg. Chem. 627 (2015) 294–298.

[34] H. Schäfer, R. Gruehn, F. Schulte, The Modification of Niobium Pentoxide, Angew. Chem. Int. Ed. 5 (1966) 40–52.

[35] G. Brauer, Die Oxyde des Niobs, Z. Für Anorg. Und Allg. Chem. 248 (1941) 1–31.

[36] O.F. Lopes, V.R. De Mendonça, F.B.F. Silva, E.C. Paris, C. Ribeiro, Niobium oxides: an overview of the synthesis of Nb₂O₅and its applicatio in heterogeneous photocatalysis, Quim. Nova 38 (2014) 467–472.

[37] I.E. Wachs, Raman and IR studies of surface metal oxide species on oxide supports: supported metal oxide catalysts, Catal. Today 27 (1996) 437–455.

[38] J.-M. Jehng, I.E. Wachs, Structural chemistry and Raman Spectra of niobium oxide, Chem. Mater. 3 (1991) 100–107.

[39] J.-M. Jehng, I.E. Wachs, Molecular structures of supported niobium oxide catalysts under in situ conditions, J. Phys. Chem. 95 (1991) 7373–7379.

[40] A.A. Mcconnell, J.S. Aderson, C.N.R. Rao, Raman spectra of niobium oxides, Spectrochim. Acta Part A Mol. Spectrosc. 32 (1976) 1067–1076.

[41] A. Darlinski, J. Halbritter, Angle-resolved XPS studies of oxides at NbN, NbC, and Nb surfaces, IEEE Trans. Magn. 23 (2003) 1381–1384.

[42] A. Darlinski, J. Halbritter, On angle resolved x-ray photoelectron spectroscopy of

oxides, serrations, and protusions at interfaces, J. Vac. Sci. Technol. A 5 (1987) 1235–1240.

[43] C.D. Wagner, W.M. Riggs, L.E. Davis, J.F. Moulder, G.E. Muilenberg (Eds.), Handbook of X-Ray Photoelectron Spectroscopy, Perkin Elmer Corporation, Minnesota, 1979.

[44] D.D. Sarma, C.N.R. Rao, XPES studies of oxides of second- and third-row transition metals including rare earths, J. Electron Spectrosc. Relat. Phenom. 20 (1980) 25–45.

[45] A. Mozalev, R.M. Vázquez, C. Bittencourt, D. Cossement, F. Gispertguirado, E. Llobet, H. Habazaki, Formation–structure–properties of niobium-oxide nanocolumn arrays via self-organized anodization of sputter-deposited aluminum-on-niobium layers, J. Mater. Chem. C Mater. Opt. Electron. Devices 2 (2014) 4847–4860.

[46] R. Caillat, R. Fontaine, L. Feve, M.J. Guittet, Electron spectrometry (ESCA) study of electron binding energy in metallic niobium and oxides NbO, NbO₂ and Nb₂O₅, C. R. Hebd. Seances Acad. Sci., Ser. C 280 (1975) 189–191.

[47] N. Usha, R. Sivakumar, C. Sanjeeviraja, M. Arivanandhan, Niobium pentoxide (Nb₂O₅) thin films: rf Power and substrate temperature induced changes in physical properties, Opt. – Int. J. Light Electron. Opt. 126 (2015) 1945–1950.

[48] Ö.D. Coşkun, S. Demirel, G. Atak, The effects of heat treatment on optical, structural, electrochromic and bonding properties of Nb₂O₅ thin films, J. Alloys Compd. 648 (2015) 994–1004.

[49] Y. Zheng, K. Li, H. Wang, Y. Wang, D. Tian, Y. Wei, X. Zhu, C. Zeng, Y. Luo, Structure dependence and reaction mechanism of CO oxidation: A model study on macroporous CeO₂ and CeO₂-ZrO₂ catalysts, J. Catal. 344 (2016) 365–377.

[50] F. Larachi, J. Pierre, A. Adnot, A. Bernis, Ce 3d XPS study of composite CeₓMn₁₋ₓO₂₋ᵧ wet oxidation catalysts, Appl. Surf. Sci. 195 (2002) 236–250.

[51] K. Min, E.D. Park, M.K. Ji, J.E. Yie, Manganese oxide catalysts for NOₓ reduction with NH₃ at low temperatures, Appl. Catal. A Gen. 327 (2007) 261–269.

[52] E.S. Ilton, J.E. Post, P.J. Heaney, F.T. Ling, S.N. Kerisit, XPS determination of Mn oxidation states in Mn (hydr)oxides, Appl. Surf. Sci. 366 (2016) 475–485.

[53] M.C. Biesinger, L.W.M. Lau, A.R. Gerson, R.S.C. Smart, Resolving surface chemical states in XPS analysis of first row transition metals, oxides and hydroxides: Sc, Ti, V, Cu and Zn, Appl. Surf. Sci. 257 (2010) 887–898.

[54] V.P. Santos, M.F.R. Pereira, J.J.M. Órfão, J.L. Figueiredo, The role of lattice oxygen on the activity of manganese oxides towards the oxidation of volatile organic compounds, Appl. Catal. B Environ. 99 (2010) 353–363.

[55] Q. Tang, L. Jiang, J. Liu, S. Wang, G. Sun, Effect of surface manganese valence of manganese oxides on the activity of the oxygen reduction reaction in alkaline media, ACS Catal. 4 (2014) 457–463.

[56] E.R. Stobbe, D. Boer, J.W. Geus, The reduction and oxidation behaviour of manganese oxides, Catal. Today 47 (1999) 161–167.

[57] F. Kapteijn, L. Singoredjo, A. Andreini, J.A. Moulijn, ChemInform abstract: activity and selectivity of pure manganese oxides in the selective catalytic reduction of nitric oxide with ammonia, Cheminform 3 (1994) 173–189.

[58] F. Wang, H. Dai, J. Deng, G. Bai, K. Ji, Y. Liu, Manganese oxides with rod-, wire-, tube-, and flower-like morphologies: highly effective catalysts for the removal of toluene, Environ. Sci. Technol. 46 (2012) 4034–4041.

[59] B. Faure, P. Alphonse, Co–Mn-oxide spinel catalysts for CO and propane oxidation at mild temperature, Appl. Catal. B Environ. 180 (2016) 715–725.

[60] Y. Zheng, K. Li, H. Wang, D. Tian, Y. Wang, X. Zhu, Y. Wei, M. Zheng, Y. Luo, Designed oxygen carriers from macroporous LaFeO₃ supported CeO₂ for chemical-looping reforming of methane, Appl. Catal. B Environ. 202 (2017) 51–63.

[61] R. Kodama, Y. Terada, I. Nakai, S. Komaba, N. Kumagai, Electrochemical and in situ XAFS-XRD investigation of Nb₂O₅ for rechargeable Lithium batteries, J. Electrochem. Soc. 153 (2006) A583.

[62] A.M. Stoneham, P.J. Durham, The ordering of crystallographic shear planes: theory of regular arrays, J. Phys. Chem. Solids 34 (1973) 2127–2135.

[63] S. Mrowec, On the defect structure in nonstoichiometric metal oxides, Ceramurg. Int. 4 (1978) 47–58.

[64] J.S. Anderson, J.M. Browne, A.K. Cheetham, R. Von Dreele, J.L. Hutchison, F.J. Lincoln, D.J.M. Bevan, J. Straehle, Point Defects and Extended Defects in Niobium Oxides, Nature 243 (1973) 81–83.

[65] J.F. Marucco, Thermodynamic study of the system NbO₂-Nb₂O₅ at high temperature, J. Solid State Chem. 10 (1974) 211–218.

[66] T. Kikuchi, M. Goto, Oxygen vacancies in Nb₂₂O₅₄₋ₓ, Nb₂₅O₆₂₋ₓ, and Nb₂₈O₇₀₋ₓ, J. Solid State Chem. 16 (1975) 363–371.

[67] S. Iijima, S. Kimura, M. Goto, Direct observation of point defects in Nb₁₂O₂₉ by high-resolution electron microscopy, Acta Crystallogr. 29 (1973) 632–636.

[68] S. Iijima, S. Kimura, M. Goto, High-resolution microscopy of nonstoichiometric Nb₂₂O₅₄ crystals: point defects and structural defects, Acta Crystallogr. Sect. A Found. Crystallogr. 30 (2010) 251–257.

[69] R.F. Janninck, D.H. Whitmore, Electrical conduction in nonstoichiometric α-Nb₂O₅, J. Chem. Phys. 37 (1962) 2750–2754.

[70] J.F. Marucco, Electrical resistance and defect structure of stable and metastable phases of the system Nb₁₂O₂₉–Nb₂O₅ between 800 and 1100 °C, J. Chem. Phys. 70 (1979) 649–654.

[71] B. Puértolas, A. Smith, I. Vázquez, A. Dejoz, A. Moragues, T. Garcia, B. Solsona, The different catalytic behaviour in the propane total oxidation of cobalt and manganese oxides prepared by a wet combustion procedure, Chem. Eng. J. 229 (2013) 547–558.

[72] B. Solsona, T.E. Davies, T. Garcia, I. Vázquez, A. Dejoz, S.H. Taylor, Total oxidation of propane using nanocrystalline cobalt oxide and supported cobalt oxide catalysts, Appl. Catal. B Environ. 84 (2008) 176–184.

[73] O.V. Buyevskaya, M. Baerns, Catalytic selective oxidation of propane, Catal. Today 42 (1998) 315–323.

[74] M. de Dompablo, Y.L. Lee, D. Morgan, First Principles Investigation of Oxygen Vacancies in Columbite MNb2O6 (M = Mn, Fe, Co, Ni, Cu), Chem. Mater. 22 (2010) 906–913.